Conceptual Design of an eVTOL Air Shuttle for Rapid Intercity Transport

Jianqiao Xiao
ECE Department
University of Illinois
Urbana, IL 61801
Email: jxiao14@illinois.edu

Noah Salk
ECE Department
University of Illinois
Urbana, IL 61801
Email: noahs2@illinois.edu

Kiruba Haran
ECE Department
University of Illinois
Urbana, IL 61801
Email: kharan@illinois.edu

***Abstract*—This paper proposes an electric vertical take-off and landing (eVTOL) aircraft for transportation between cities separated by a short distance (<200 miles). The aircraft will carry 10 passengers and is meant to replace shuttle buses as a faster and more direct form of transportation. An iterative optimization method of developing aero-propulsive parameters for the air shuttle is proposed and demonstrated. Results of the optimization are analyzed to determine developments in enabling technology that are necessary for increasing the feasibility of this new form of transportation.**

NOMENCLATURE

η_p	Propeller Efficiency, 75%
ρ	Air Density, kg/m^3
AR	Aspect Ratio
b	Span, m
BS	Blow Span Ratio
c	Chord Length, m
C_D	Drag Coefficient
C_L	Lift Coefficient
E	Energy, kWh
e	Oswald Efficiency, 0.8
P	Power, kW
q	Dynamic Pressure, N/m^2
r	Propeller Radius, m
RC	Rate of Climb, m/s
S	Wing Area, m^2
SE	Specific Energy, kWh/kg
SP	Specific Power, kW/kg
T	Thrust, N
t	Time, s
v	Velocity, m/s
W	Weight, kg
W/P	Power Loading, kg/kW
W/S	Wing Loading, kg/m^2

I. INTRODUCTION

This paper begins by stating the motivation behind the eVTOL aircraft concept as well as providing examples of existing proposed designs. It follows by introducing the configuration and mission profile of our proposed aircraft. The iterative design flow of a VTOL aircraft is then discussed along with the method used to achieve an optimal design for a given objective. By looping through mission profiles with various ranges, we explore shifts in maximum payload versus range curves under various improvements in battery technology. Results from a fixed maximum take-off weight (MTOW) optimization uncovers the trade-offs between required cruise energy, wing surface area, and wing aspect ratio. Next, two specific cases are studied to show how an increase in electric motor specific power past the state-of-the-art (SOA) may result in better aircraft performance. A feasible design that meets the desired mission profile requirements is specified at the end of the paper.

II. BACKGROUND

Due to the vast landscape of the United States, fast transportation between city hubs is challenging. In particular, for transits that take around two hours by car, there currently exists no perfect method of getting from point A to point B. Railroads are owned by freight companies that take priority over commercial trains, resulting in large delay times. High speed rail is a good option for smaller countries, but for a country like the United States, the overhead infrastructural cost for an effective high speed rail network is prohibitive [1]. The shuttle bus is another form of transportation that's too slow, inconvenient, polluting, and arguably unsafe. Regional jets may not save much time for this particular mission because of the placement of airports outside city centers as well as airport processes which combine to significantly increase transit time.

A method of rapid intercity transport is in demand by frequent travelers. Business people may want to attend a meeting in a nearby city and immediately return to work; students and academics may need to visit another campus for research collaboration and return to campus shortly afterwards. However, for cities separated by about 200 miles, traveling between the two becomes loathsome due to a nearly five hour round-trip transit time for any current form of transportation.

In order to improve intercity transportation, the University of Illinois recently launched the UI Ride shuttle service from Urbana-Champaign campus to Chicago campus aiming to support research and teaching collaboration [2]. Yet, travellers still need to spend three hours on the road before reaching their destination. As the technologies behind motors, batteries, and

Fig. 1. Similar eVTOL Designs: EHANG (top-left), Aurora PAV (top-right), and Lilium (bottom)

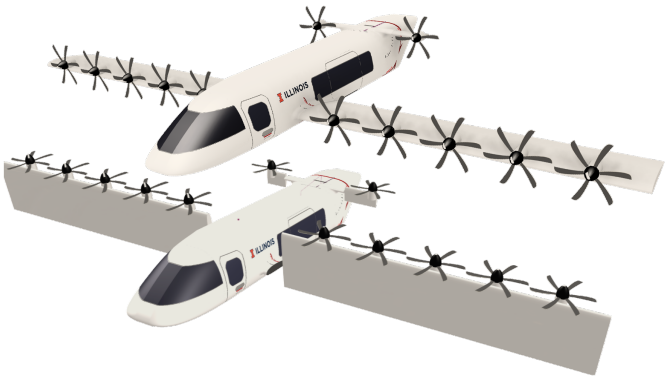

Fig. 3. CAD model of the proposed design (top and bottom are in cruise and VTOL configurations respectively)

power systems evolve, eVTOL aircraft have the potential of accelerating intercity transportation.

An eVTOL aircraft is one solution to the transportation problem due to its fast flight speed and agility when taking off and landing in a complex downtown environment. Manned eVTOL aircraft designs proposed in the past can be roughly classified into the following three categories. The multi-rotor configuration includes several lifting fans that both elevate and propel the vehicle; the lift-and-cruise aircraft use lifting fans only during take-off and landing and use fixed wings during cruise; the tilt-rotor vehicle whose wings and propellers can tilt for best take-off/landing and cruise performance. One example from each category is shown in the following paragraphs.

Ehang 184, in the multi-rotor category, is lifted by four counter-rotating propellers. The vehicle carries one person and can fly at 100 km/h for twenty-five minutes, covering approximately 40 km [3].

Aurora PAV belongs to the lift+cruise category. It has eight lifting fans, one horizontal propeller and a fixed wing. This design carries two people and flies at 180 km/h for 80 km [4].

Lilium, a tilt-wing design, consists of thirty-six electric fans distributed along the tilt wings and tilt canards. This design carries two people and flies at 280 km/h for 300 km [5].

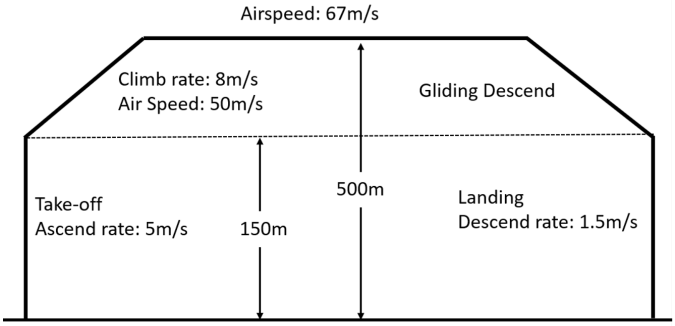

Fig. 2. Typical Mission Profile

III. Proposed Idea

We propose an eVTOL air shuttle that carries ten people, covers 200 km, and can take-off and land in a parking lot. The mission profile and vehicle design space will be discussed in this section. The mission profile of the proposed design is shown in Fig. 2. The vehicle takes off vertically from a parking lot or open area and lifts to reach a minimum building clearance of 150 meters at an ascend rate of 5 m/s (typical for a helicopter [6]). The wings and propellers then tilt forward to transform the aircraft into a horizontal climb at a vertical climb velocity of 8 m/s and an airspeed of 50 m/s. At an altitude of 500 m, the vehicle flat lines to cruise at 67 m/s towards the final destination. The aerodynamic flight portion of the mission profile mimics that of a similarly sized conventional aircraft. The Beechcraft Queen Air 65 is used as a baseline not just for airspeed and climbing rate references, but also for the component weight breakdown that is used in the optimization. The abundance of information on this aircraft [7] increases the fidelity of our design. On approach, the air shuttle will initiate a powerless, gliding descent until reaching an altitude of 150 m. It then transforms into a vertical landing configuration with propellers tilted upwards until touchdown. The vertical descent rate of 1.5 m/s is chosen by considering passenger comfortability and typical helicopter performance [8]. This is important because VTOL speeds have a large impact on the total mission energy requirement and, as a result, the feasibility of the vehicle topology.

The design adopts a multi-propeller tilted rotor-wing design as shown in Fig. 3. The tilt mechanism enables VTOL capabilities while maintaining a good cruise efficiency. During take-off and landing, the wings with propellers rotate towards a vertical position and the vehicle hovers as a multi-rotor vehicle. During climb and cruise, the wings rotate towards a horizontal position and the vehicle uses its airfoils to provide aerodynamic lift. The aspect ratio AR, the number of propellers N, and the fraction of the span under the blown-span effect BS are selected to be the design variables in the initial sizing.

IV. Sizing Process

A. Baseline Aircraft

To support weight estimations throughout the sizing process, a baseline aircraft's mass breakdown was used to form a constant weight component for all vehicle designs. Fuselage, landing gear, avionic + instrumentation, propeller, electrical system, air-conditioning, and furnishing masses were extracted from the Beechcraft 65 Queen Air to comprise, W_{const}, an unchanging structural and auxiliary weight. The Beechcraft 65QA is a twin-engine fixed wing general aviation aircraft with a carrying capacity of 9-10 people. It has a very similar operational profile to our proposed design and is therefore selected to be the baseline aircraft for this study. Also taken from the 65QA is the wing mass per unit surface area, σ_{wing}, used in the weight estimation loop to calculate wing mass at a given wing loading. Data extracted from the baseline aircraft is listed in Table I.

TABLE I
Beechcraft 65QA Mass Decomposition

Item	Value
Fuselage	275 kg
Landing Gear	200 kg
Avionics + Instrum.	32 kg
Propeller	117 kg
Electrical System	75 kg
A/C	40 kg
Furnishing	200 kg
Total Fixed	822 kg
Wing Density, σ_{wing}	11.14 kg/m^2

TABLE II
Design Space Boundaries

Parameter	Minimum	Maximum	Type
AR (x_1)	4.5	15	Linear
N/2 (x_2)	2	30	Integer
BS (x_3)	0.05	0.95	Linear

B. Genetic Algorithm Optimization

A genetic algorithm (GA) based optimization tool, GOSET, is used in various applications throughout this study. A flowchart of the optimization scheme is shown in Fig. 4 and the design variables are shown from a top-view of the aircraft in Fig. 5. Each individual design (or gene) has a unique combination of the three variable: aspect ratio (AR), half of the total number of propulsors (N/2), and the ratio of the wing span swept by propellers (BS). Each variable has a minimum and maximum possible value based on a feasible design space boundary, defining a range from which the algorithm can randomly choose design points. Only the N/2 variable is constrained to an integer value, while the others are linear within their respective range. Information on each design variable is given in Table II.

An initial population of 300 individuals is generated and each design is run through an iterative sizing process. Wing loadings are swept up to the stall constraint for every design and the maximum payload that vehicle can handle under the given wing loading while remaining at or below an MTOW of 2500 kg [9] is estimated through a weight iteration. The gene fitness is evaluated based upon the maximum achievable payload over all best designs for each wing loading. Based on the fitness of each individual the algorithm chooses which genes to kill and which to mutate in order to maximize the fitness value for the next generation. In total, there are 35 generations and each consecutive generation after the initial population contains 100 individuals. Information on every design is recorded for post-processing.

C. Mission Profile and Power Loading Constraint Curves

For each optimization, a set of mission profile defining parameters are loaded with information that contains velocities, distances, altitudes, as well as calculated air densities for each of the flight profile's five segments. To aid in the sizing iteration, aircraft designers typically use power loading versus wing loading constraint curves which depict the rated power of the vehicle's power plant and wing surface area as they are inversely normalized to the aircraft's total weight [10]. This is useful because while we hold the wing loading and corresponding power loading constant throughout the iteration, the total power demand and wing surface area requirement become a function of only the vehicle's total weight.

Constraint curves are dependent on the mission profile and vary greatly with each flight phase. Equations 1-5 give the expressions used to calculate constraint curves during cruise and climb. The approach constraint is a vertical line at the wing loading corresponding to stall speed as we assume a gliding, powerless descent [11].

$$k = \frac{1}{\pi e AR} \tag{1}$$

$$q = \frac{1}{2}\rho v^2 \tag{2}$$

$$(T/W)_{cruise} = \frac{g}{1000}\left(\frac{qC_{D0}}{W/S} + k\frac{W/S}{q}\right) \tag{3}$$

$$(T/W)_{climb} = \frac{g}{1000}\left(\frac{RC}{v} + \frac{qC_{D0}}{W/S} + k\frac{W/S}{q}\right) \tag{4}$$

$$P/W = \frac{(T/W)v}{\eta_p} \tag{5}$$

For each design in the optimization, a new set of curves are generated and overlaid with each other. For any wing loading, the vehicle must be sized for the minimum power loading amongst all flight phases. Constraints for the VTOL portion of the mission are horizontal lines at the power loading corresponding to the maximum power condition (VTOL). This constraint curve, however, is not considered during the sizing of the motor or power electronics as we assume a short-time overload of both components. The vertical take-off portion of the mission profile lasts for about 30 seconds while the vertical landing segment lasts for 100 seconds. The ability of the machine and power electronics to withstand overloading conditions for this short period of time is an area for future work in each respective discipline.

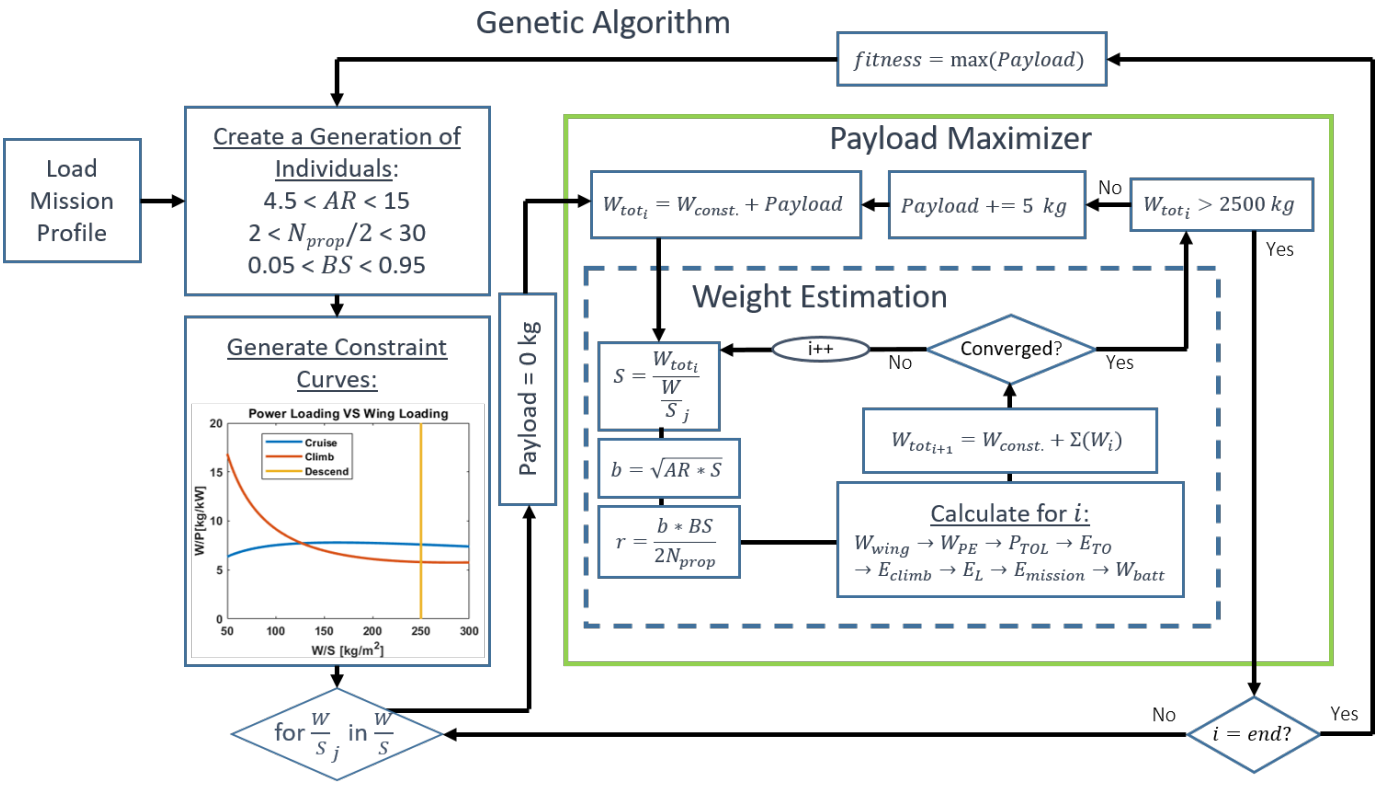

Fig. 4. Optimization flowchart

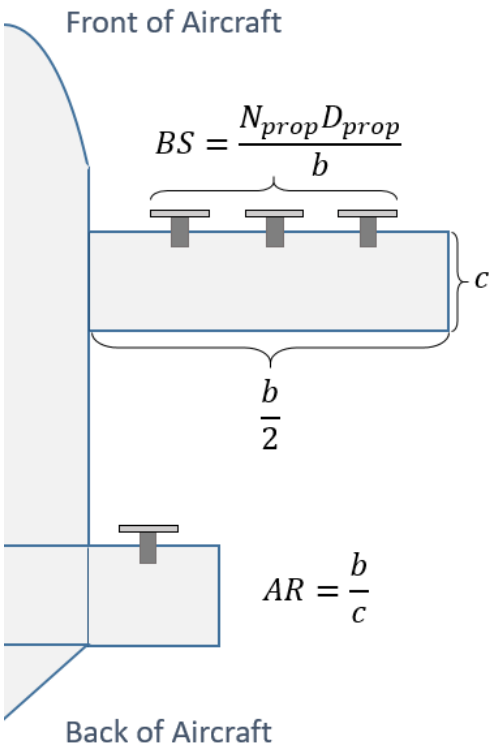

Fig. 5. Top view of vehicle layout with parameters to be optimized

D. Weight Estimation

Because component weights are dependent on the MTOW (through proxy of power loading, wing loading, and mission energy), it is an iterative process to determine the final vehicle weight. To kick start the iteration, an initial MTOW estimate is made using the sum of W_{const} and the current payload. The current payload starts off as 0 kg but is incremented upon convergence until the desired MTOW is reached. The following equations were used in the weight estimation loop for iterate i and wing loading j [12], [13]:

$$S_i = \frac{W_{tot_i}}{(W/S)_j} \tag{6}$$

$$b_i = \sqrt{AR \cdot S_i} \tag{7}$$

$$r_i = \frac{b_i \cdot BS}{2N_{prop}} \tag{8}$$

$$P_{TOL_i} = \frac{N_p}{\eta_p} \sqrt{\frac{(W_{tot_i} g)^3}{2N^3 \rho \pi r_i^2}} \tag{9}$$

$$[E_{TO_i},\ E_{L_i}] = \frac{[t_{TO},\ t_L] P_{TOL_i}}{3600000} \tag{10}$$

$$E_{climb_i} = \frac{W_{tot_i} t_{climb}}{3600 (W/P)_{climb_j}} \tag{11}$$

$$E_{cruise_i} = \frac{W_{tot_i} t_{cruise}}{3600 (W/P)_{cruise_j}} \tag{12}$$

$$W_{wing_i} = \sigma_{wing} S_i \tag{13}$$

$$W_{PE_i} = \frac{W_{tot_i}}{\min((W/P)_{climb_j}, (W/P)_{cruise_j}) \cdot SP_{PE}} \tag{14}$$

$$W_{M_i} = \frac{W_{tot_i}}{\min((W/P)_{climb_j}, (W/P)_{cruise_j}) \cdot SP_{M}} \tag{15}$$

$$W_{b_i} = \max(\frac{P_{TOL_i}}{SP_b}, \frac{E_i}{SE_b}) \tag{16}$$

$$W_{tot_{i+1}} = W_{const} + \Sigma W_i \tag{17}$$

Depending on the wing and power loading the iteration will either converge or grow unbounded. To account for unstable design points the number of iterations is limited to 100 and if the design has not converged by the last iteration it is killed by assigning a maximized payload of zero. If the design point converged but the MTOW is less than 2500 kg the payload is incremented by 5 kg and the iteration process starts over again with this new payload. Once the MTOW exceeds 2500 kg, the sizing is complete and must pass feasibility evaluations which enforces the wingspan and propeller radius to be less than 19 meters and 0.75 meters respectively. The design is killed if these limits are violated, otherwise it is left alone; finally, we move to the next wing loading.

V. Optimization Results and Discussion

The results of two separate optimizations are discussed in this section. Fig. 6 demonstrates the trade-off between payload capacity and range of the eVTOL, and the potential shifts in performance through the advancement of battery technology, while Fig. 7 reveals the impact of a high aspect ratio on the total energy consumed during the cruise segment, which accounts for a large portion of the vehicle's total energy expenditure.

A. Payload vs. Range

By performing a looped GA optimization and sweeping through mission profile ranges from 100-500 km, the maximum achievable payload at any given design range is obtained. As fidelity of the results is largely determined by a desired run-time, the curves in Fig. 6 show general trends for the SOA (shown in red) and for various improvements in battery technology. To simulate "modest" advancements in energy storage, three additional scenarios were explored with:

1) Double SOA in battery specific power [14] (Green)
2) Double SOA in battery specific energy [14] (Blue)
3) Double SOA of both specific power and energy (Black)

The general structure of each curve in Fig. 6 is a constant maximum payload until some critical range, at which point the payload begins to drop off with increasing range. Because the maximum boundary for explored ranges was set to 500 km, it is assumed that the critical range for the 1 kWh/kg, 1 kW/kg case is greater than 500 km and that the critical range for the 0.5 kWh/kg, 2 kW/kg case happens prior to 150 km, before which it flat-lines at the same maximum payload as the 1 kWh/kg, 2 kW/kg case. It is also interesting to note that the general slope of the drop-offs for each case appears to happen at the same rate.

It can be seen that the global maximum for any given state of technology is constrained by the battery specific power. The critical range can be explained through Eq. 16. As battery weight accounts for a significant portion of the vehicle's MTOW (~30%), any shifts or discontinuities in the battery weight will greatly impact the maximum payload achievable for a given design. Battery weight is calculated by the worst case scenario of power demand (which happens during VTOL) and energy demand (largely comprised of cruise energy requirements and is thus dependent on range). Therefore, it is determined that battery weight and MTOW are contingent upon the power demand prior to the critical range, as in this region battery weight has no dependence on range. After the critical range, battery weight and MTOW are indirectly dependent on range through an increase in total mission energy requirements.

B. Energy Storage

Throughout this paper, it is assumed that the energy storage element of choice is a battery. However, the results of the optimization are valid for any form of energy storage. Fuel cells offer higher specific energy than batteries but lag behind in the area of specific power [15]. There is also potential for future studies to explore combinational energy storage. For example, to compensate for the relatively poor specific power of fuel cells, pre-charged ultracapacitors can be used to service high power demands during vertical take-off and can then be trickle charged during cruise by fuel cells for vertical landing. The feasibility of this approach is determined by VTOL energy demands and whether or not ultracapacitors can supply this high load for the entirety of the mission profile's vertical flight segments. In future studies, energy storage densities should be compared with volumetric constraints in the sizing loop to validate the feasibility of a design.

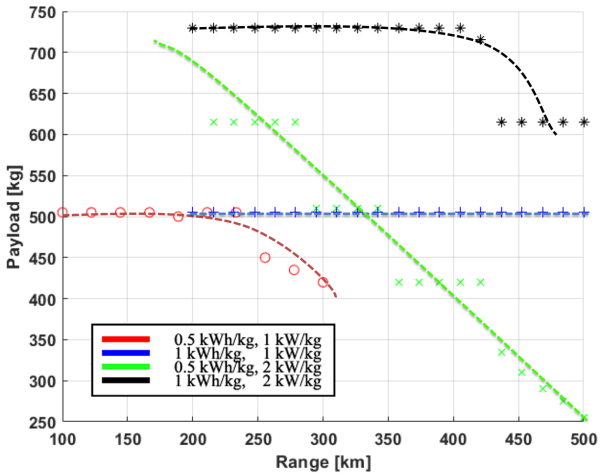

Fig. 6. Payload vs range with various battery technology improvements, MTOW = 2500 kg

C. Wing Area and Cruise Energy's Variance with Aspect Ratio

A larger aspect ratio is sometimes preferred for distributed propulsion aircraft because it may reduce the induced drag and allow more space to install a distributed array of propulsors [16]. However, by simultaneously plotting the energy consumed during cruise and wing area against the aspect ratio, as shown in Fig. 7, a clear trend appears that cruise energy consumption increases with aspect ratio. Since the cruise energy consumption contributes only to the thrust that counteracts the aerodynamic drag, the drag increases as the aspect ratio increases. The wing area is plotted against aspect ratio in order to show the change in lift coefficient, C_L. In Fig. 7, the blue line shows the decrease in wing area as the aspect ratio increases. Since the total weight equals the lift force, a decrease in wing area results in a higher wing loading and therefore a higher lift coefficient as described in Eq. 18:

$$C_{Di} \propto C_L^2,\ C_{Di} \propto \frac{1}{AR} \tag{18}$$

This equation relates the induced drag coefficient's proportional dependence on the lift coefficient and aspect ratio. The lift coefficient has a much stronger influence on induced drag than the aspect ratio does and therefore any increase in AR will result in larger energy consumption during cruise.

VI. Electric Motor Case Studies

Two cases were studied to explore potential changes in the vehicle design specifications as the motor specific power increases. The first case considers a motor with specific power of 5 kW/kg as the sole provider of propulsive power; this is the current SOA for electric machines with mature technology readiness levels [17]. The second case assumes a motor specific power of 15 kW/kg: a value achievable in the near future [18]. For each case, the optimization is applied to maximize payload and minimize battery mass. Fig. 8 shows the location of each case's optimized design as they lie on the constraint curves. It can be seen that advancements in motor technology take the load requirement off of the wings and provide an excess of power during flight phases that require more lift. This means that the design can now be sized for cruising conditions with a lower wing loading. Specifications for each case are shown in Table III. Though the assumed motor specific power is tripled from Case 1 to Case 2, the maximum payload only increases by 10 kg, a 2% improvement. This indicates that propulsor specific power advancements may not play a large roll in pushing payload capacities. However, it should be noted that the battery mass and total mission energy requirement decreased by 8.7% and 24.2% respectively from Case 1 to Case 2. These are major considerations when estimating the vehicles material, operational, and maintenance costs.

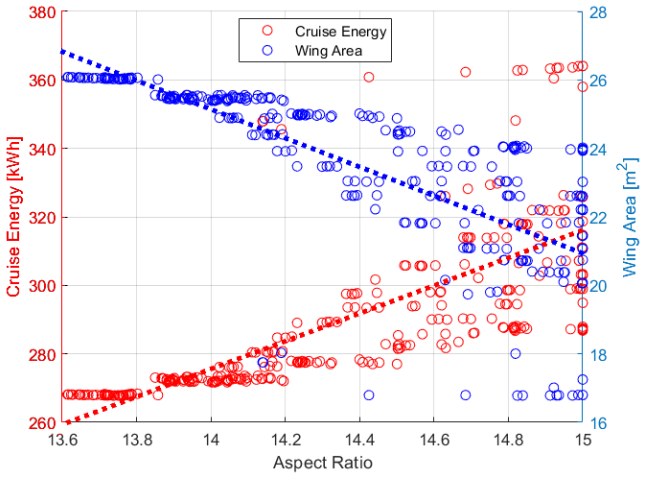

Fig. 7. The effect of aspect ratio on wing area and cruise energy

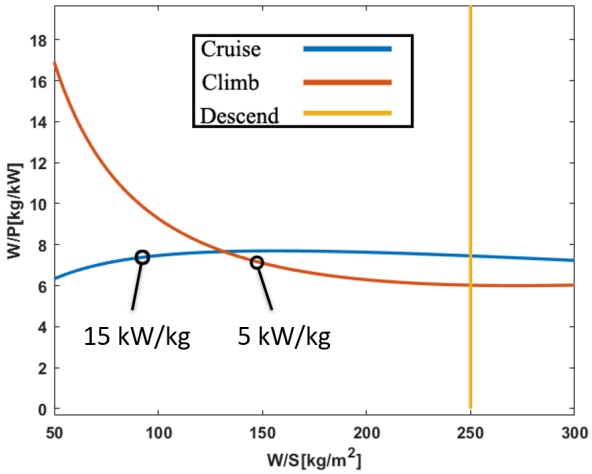

Fig. 8. Constraint curves for the best design in each case (maximized payload)

VII. Final Proposed Design

The optimization method used to maximize payload for a given MTOW was tweaked to minimize MTOW for a given payload. The payload was set to 1000 kg to give us an optimal result for the desired ten-passenger air shuttle. The GA fitness function was adjusted accordingly. The optimal design's specifications are given in Table IV.

TABLE III
Case Study Results with Varying Motor Specific Power

Item	Case 1: 5 kW/kg	Case 2: 15 kW/kg
Total Mass [kg]	2500	2500
Aspect Ratio	14.5	13.8
Wing Area [m^2]	17	26
Number of Propellers	10	12
Radius of Propeller	0.74	0.74
Payload [kg]	500	510
Wing loading [kg/m^2]	147	96.4
Motor Mass [kg]	70.86	22.4
Battery Mass [kg]	785	717
Total Energy [kWh]	392	297
Power Overload Factor	2.22	2.13

TABLE IV
PROPOSED DESIGN SPECIFICATIONS

Item	Value
Transit Time [min]	64
Total Mass [kg]	3575
Aspect Ratio	13.7
Wing Area [m^2]	26.12
Number of Propellers	12
Radius of Propeller	0.75
Payload [kg]	1000
Wing Loading [kg/m^2]	136.9
Total Energy [kWh]	537
Motor Specific Power [kW/kg]	10
Motor Mass [kg]	95.4
Power Overload Factor	1.28

The proposed design result is compared with the 5 kW/kg, 500 kg payload case in Table III and the following discoveries are made:

1) The payload of the proposed ten-passenger aircraft sees an increase of 100%, but the MTOW only increases by 43%. This emphasizes the importance of the proposed optimization method, as aircraft sizing clearly does not scale proportionally.
2) The total energy consumption of the proposed design sees an increase of 37% while the battery weight increases by 55%. Since our battery is sized so that both power and energy requirements are satisfied, the specific power appears to be the limiting factor when determining the battery weight.

Table V gives a mass breakdown of the final design.

VIII. CONCLUSION AND FUTURE WORK

This study identified a gap in transportation for ranges from 200 to 300 km. To fill this void, the design space of a new form of mid-range electric aircraft was explored. The results of the study point toward improvements in enabling technologies required to usher in eVTOL and Urban Air Mobility prevalence.

The optimization was adjusted to generate a high-level depiction on the trade-offs between range and payload for various energy storage performance improvements over the SOA. The effect of increasing electric motor specific power was explored and it was determined that while this may not impact the maximum achievable payload, it may result in less mission energy requirements, battery weight, and consequently overall vehicle cost. After an exercise to maximize the payload for a given MTOW, the proposed concept was optimized for a desired payload of 1000 kg to support 10 passengers. Improvements upon the proposed model and method of optimization will be the focus of future work and can be refined in the following ways:

1) An assumption in this study is that energy storage is supported by only batteries. Future work should focus on exploring alternative energy storage elements and the potential of combining them to match the demands of each flight phase. Energy densities should be taken into account to validate that the design passes volumetric constraints.
2) Though the design proposed in this paper utilizes distributed propulsion, the benefit of the blown-wing effect is not currently captured in the constraint curves calculations. An extra iteration should be performed to include the change in lift coefficients and slip stream conditions [19].
3) For a mono-planar design, the wing area, aspect ratio and number of propellers are optimized. However, the vehicle profile is still considerably large with an 18-meter wing span. Methods to decrease the vehicle's footprint should be considered for better maneuverability within cities. A double-wing design can reduce the span, but imposes challenges for aerodynamic modelling of the vehicle.
4) Higher fidelity in vehicle weight estimations can be achieved by accounting for the tilt-wing mechanism, battery infrastructure, structural weight as a function of wing span, and modern composites.
5) This paper assumes a motor overload of 1.2-2.3x rated power during VTOL, which typically lasts for less than two minutes. As traditional OEMs prefer air-cooled motors, further investigations will be made into the ability of different motor types to handle overloading conditions. Aggressive, lightweight heatsinks will be explored to more effectively extract losses from the conductors.

TABLE V
PROPOSED DESIGN MASS DECOMPOSITION

Item	Mass	%
Wing [kg]	291.0	8.1
Power Electronics [kg]	31.8	0.9
Motor [kg]	95.4	2.7
Battery [kg]	1217.7	34.1
Payload [kg]	1000	28.0
Fixed [kg]	822	23.0
Propeller [kg]	117	3.2
Total [kg]	3574.9	100

REFERENCES

[1] H. Glickenstein, "High-speed rail for the united states? [transportation systems," *IEEE Vehicular Technology Magazine*, vol. 4, no. 3, p. 16–23, 2009.
[2] L. Velazquez, "Shuttle service connects UI, Chicago campuses," *The Daily Illini*, Sep 2019.
[3] EHANG, INC. Redwood City, CA, "Multi-rotor aircraft.," 2018.
[4] "Aurora Flight Sciences PAV," *Electric VTOL News*, 2019.
[5] D. Grossman, "Germany's Air Taxi Takes Flight," *Popular Mechanics*, Oct 2019.
[6] J. W. R. Taylor, *Janes all the worlds aircraft: 1988-89*. Janes Information Group, 1988.
[7] J. Roskam, *Airplane design*, vol. 5. DARcorporation, 2018.
[8] F. A. ADMINISTRATION, *Helicopter Flying Handbook*. FAA, 2012.
[9] AIAA and IEEE, "Aiaa/ieee eats students design challenge 2020."
[10] E. Torenbeek, *Synthesis of subsonic airplane design: an introduction to the preliminary design of subsonic general aviation and transport aircraft, with emphasis on layout, aerodynamic design, propulsion and performance*. Delft University Press, 1988.

[11] F. Orefice, P. D. Vecchia, D. Ciliberti, and F. Nicolosi, "Aircraft conceptual design including powertrain system architecture and distributed propulsion," *AIAA Propulsion and Energy 2019 Forum*, 2019.
[12] B. W. McCormick, *Aerodynamics Aeronautics and Flight Mechanics*. John Wiley & Sons, 1995.
[13] M. Tyan, N. V. Nguyen, S. Kim, and J.-W. Lee, "Comprehensive preliminary sizing/resizing method for a fixed wing – vtol electric uav," *Aerospace Science and Technology*, vol. 71, p. 30–41, 2017.
[14] A. Khaligh and Z. Li, "Battery, ultracapacitor, fuel cell, and hybrid energy storage systems for electric, hybrid electric, fuel cell, and plug-in hybrid electric vehicles: State of the art," *IEEE Transactions on Vehicular Technology*, vol. 59, no. 6, p. 2806–2814, 2010.
[15] T. Kadyk, C. Winnefeld, R. Hanke-Rauschenbach, and U. Krewer, "Analysis and design of fuel cell systems for aviation.," *Energies (19961073)*, vol. 11, no. 2, p. 375, 2018.
[16] H. D. Kim, A. T. Perry, and P. J. Ansell, "A review of distributed electric propulsion concepts for air vehicle technology," *2018 AIAA/IEEE Electric Aircraft Technologies Symposium*, Aug 2018.
[17] X. Zhang, C. L. Bowman, T. C. Oconnell, and K. S. Haran, "Large electric machines for aircraft electric propulsion," *IET Electric Power Applications*, vol. 12, p. 767–779, Jan 2018.
[18] A. Yoon and K. Haran, "Scaling study of high frequency machine for electric aircraft propulsion," *2018 IEEE Energy Conversion Congress and Exposition (ECCE)*, 2018.
[19] R. de Vries, M. Brown, and R. Vos, "Preliminary sizing method for hybrid-electric distributed-propulsion aircraft.," *Journal of Aircraft*, vol. 56, no. 6, pp. 2172 – 2188, 2019.